Topological constraints on positions of magnetic solitons in multiply connected planar magnetic nanoelements

Andrei B. Bogatyrëv*
Institute for Numerical Mathematics, Russian Academy of Sciences, 8 Gubkina str., Moscow GSP-1, 119991 Russia

Konstantin L. Metlov†
Donetsk Institute of Physics and Technology, 72 R. Luxembourg str., Donetsk 83114, Ukraine
(Received 19 September 2016; revised manuscript received 13 November 2016; published 4 January 2017)

Here we consider an interplay between the topology of the magnetization texture (which is a topological soliton, or skyrmion) in a planar magnetic nanoelement and the topology of the element itself (its connectivity). We establish the existence of a set of constraints, coupling these topologies, which are specific for multiply connected elements and are absent in the simply connected case. As an example, a specific constraint is derived for a case of a planar ring magnet, relating the angular positions of magnetic vortices and antivortices inside. We analyze the recent experimental data on the vortex magnetic domain walls in the ring to validate our findings.

DOI: 10.1103/PhysRevB.95.024403

Planar magnetic nanoelements are currently being adopted rapidly for various applications of magnetism, most notably magnetic random access memory (MRAM) [1], spin-transfer-torque MRAM (STT-MRAM) [2], and patterned magnetic recording media [3], but also as an integral part of other spintronic devices, such as nanoscale microwave generators [4], magnetic tunnel transistors [5], racetrack magnetic memories [6], and other devices built on top of spin valves and magnetic tunnel junctions. This is mainly thanks to their compatibility with existing nanoscale patterning technologies, such as ultraviolet and E-beam lithography. They are also being studied extensively using numerical methods of micromagnetics.

Most of the present applications of planar magnetic nanoelements are based around the control, achieved by changing the nanoelement's shape and size (such as introducing/reducing the artificial anisotropy, or forcing the elements into a particular magnetic state at remanence). Significant progress was made in understanding the magnetic states of such simply connected elements. For example, the states of circular nanocylinders were studied extensively both theoretically [7–10] and numerically [11]. Manipulating the element's connectivity, however, opens a much wider avenue for control of its magnetic properties. By designing the size and shape of holes in magnetic nanoelements, it should be possible not only to change their macroscopic properties (anisotropy, susceptibility, excitation frequencies, and coercivity) but also to significantly expand the set of metastable magnetic textures in such elements and directly influence the (static or dynamic) transitions between each of these states. In other words, such a degree of control offers additional possibilities for *processing* the information within the magnetic nanostructures as opposed to merely *storing* it. There are only a few direct and detailed (with full resolution of the magnetic texture both in time and in space) experiments on multiply connected nanoelements, most notably Ref. [12], which was actually aimed at studying the impact of sample curvature on domain-wall propagation, but turns out to be very useful for elucidating the topological properties of magnetization textures.

In this work, we construct general statements about the properties of magnetization configurations in multiply connected planar magnetic nanoelements. The analytical theory of such textures appeared only recently [13]. It expresses the local magnetization in terms of analytical functions of complex variables and, in particular, the Schottky-Klein prime functions [14,15]. These functions are not easy to evaluate [16], which diminishes somewhat the value of having compact analytical expressions. However, such a representation may pave the way for symbolic analysis, making it possible to express some of the properties of magnetization textures in the form of simple constraints. These constraints have a topological nature and are directly related to the connectivity of the planar magnetic nanoelement; they are the main subject of the present work. While this consideration is approximate and the observed (measured or computed) magnetization textures may differ locally from what is predicted by our simple analytical theory, it can be hoped that an intricate interplay of the topology of the magnetization textures (which are magnetic topological solitons, or skyrmions) and the topology of the magnetic nanoelement is captured well by the present analysis.

In the following, we briefly remind the reader of the approximate mapping of the problem of the magnetization textures of planar magnetic nanoelements to the complex analysis [17], which is our starting point. Then we derive the topological constraints for the case of a doubly connected planar nanoelement (a ring). Finally, we analyze recent experimental data on the dynamics of head-to-head magnetic vortex walls in a ring [12], and we check the established constraints. We discuss the applicability of our results and draw conclusions at the end.

The defining feature of ferromagnets is the presence of nonzero local magnetic moments inside each small (but macroscopic) volume of the material. Their magnitude per unit of the material's volume is a temperature-dependent quantity called the saturation magnetization of the material (M_S), but their directions may vary. The spatial distribution of these vectors of constant length is called the magnetization texture (such as, for example, the texture with two head-to-head

*gourmet@inm.ras.ru
†metlov@fti.dn.ua

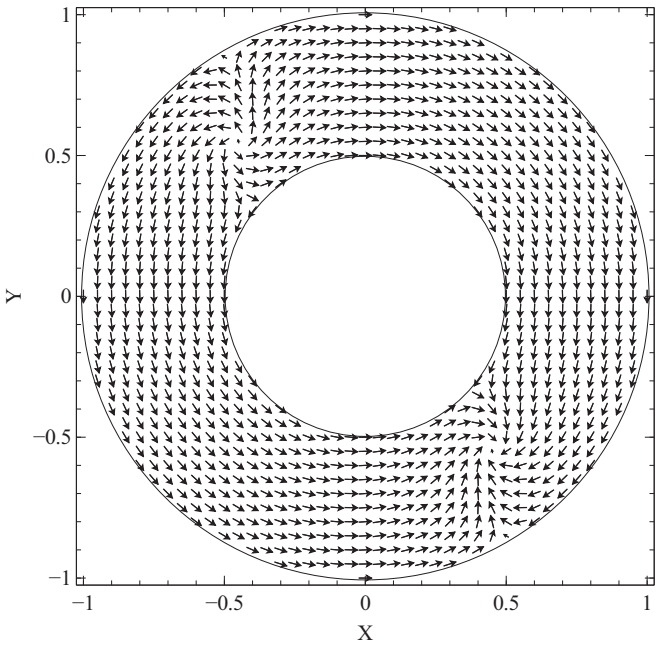

FIG. 1. The configuration of local magnetic moments (magnetization texture) in a ring, containing two 180° head-to-head vortex domain walls. The arrows correspond to the dimensionless in-plane magnetization vectors $\{m_X, m_Y\}$ plotted against the dimensionless coordinates X and Y normalized by the outer radius of the ring. The magnetization components are calculated according to (1) and (2) with $e_1 = 0.2$ and $e_2 = 2$ and the analytical expression for $f(z)$ from Ref. [13].

magnetic vortex walls in a ferromagnetic ring, shown in Fig. 1).

Typically ferromagnets of a specific size and shape can support several metastable magnetization textures at each set of external parameters, such as temperature, pressure, and the configuration of the externally applied magnetic fields. What textures may be there is the subject of micromagnetics [18,19], and, particularly for multiply connected planar nanomagnets, of the present paper. From general micromagnetics, it follows that this set is determined [18] by various interactions between the local magnetic moments, such as the exchange interaction, the magnetostatic dipolar interaction, the crystalline magnetic anisotropy, the Dzyaloshinskii-Moriya interaction, etc. In a typical soft nanomagnet (that is, around micron size or smaller) at remanence (without the external magnetic field) these interactions form a hierarchy with ferromagnetic exchange as the strongest, then the various magnetostatic energy terms, then the rest of the interactions. If the nanomagnet is planar, this hierarchy can be employed to represent a wide class of trial functions for the magnetization distributions by functions of complex variables [17]. Specifically, the trial functions are built by minimizing the energy terms sequentially from strongest to weakest, with each step building on top of the previous one and selecting the functions, which, additionally, minimize the next weaker energy term [17]. The exact solution in this picture corresponds to *simultaneous* minimization of all energy terms and is not available at the moment for the considered nonellipsoidal magnets. Nevertheless, the approximate expressions for the magnetization distributions, following from the described sequential minimization framework, are very convenient for obtaining useful closed-form analytical results, with excellent agreement with experiments [9,10,20–23].

The trial functions for the magnetization distributions in planar soft nanomagnets [17] can be written by expressing the Cartesian components of the magnetization as a stereographic projection:

$$m_X + \imath m_Y = \frac{2w}{1 + w\overline{w}},$$
$$m_Z = \frac{1 - w\overline{w}}{1 + w\overline{w}}, \tag{1}$$

where the overline denotes complex conjugation, and the Cartesian coordinate system is chosen in such a way that suitably normalized dimensionless coordinates X and Y define a point on the element's face (having an arbitrary shape $\mathcal{D}$). The elements are assumed to be thin enough so that the Z dependence of the magnetization (across the element's thickness) can be ignored. The representation ensures that the length of the reduced magnetization vector $|\vec{m}| = |\vec{M}|/M_S = 1$ is a constant at every point inside the magnet. The function $w = w(z,\overline{z})$ is a complex function of the complex variable $z = X + \imath Y$, $z \in \mathcal{D}$, which is not necessarily analytic, but it can be expressed via another analytic function $f = f(z)$ as

$$w(z,\overline{z}) = \begin{cases} f(z)/e_1, & |f(z)| \leqslant e_1, \\ f(z)/\sqrt{f(z)\overline{f}(\overline{z})}, & e_1 < |f(z)| \leqslant e_2, \\ f(z)/e_2, & |f(z)| > e_2, \end{cases} \tag{2}$$

where e_1 and e_2 are two real scalars, satisfying $0 < e_1 < e_2 < \infty$. The function $f(z)$, in turn, is the solution of the Riemann-Hilbert boundary-value problem of finding the analytic function with no normal components on the boundary of the domain $\mathcal{D}$. The solution of this boundary-value problem usually depends on a number of real and complex constants, which, together with e_1 and e_2, serve as Ritz parameters for the final magnetic energy minimization, which includes all the energy terms irrespective of their place in the hierarchy.

For example, in the simplest case of a single vortex in a circular disk, the solution of the above-specified Riemann-Hilbert problem is $f(z) = \imath zc + A - \overline{A}z^2$, with c and A being real and complex scalars, respectively [24]. It is possible to generalize this solution for the case of multivortex states [17], in which case it depends on additional scalar parameters, related to the positions of vortices and antivortices on the element's face.

For multiply connected regions, the multivortex (and antivortex) solution $f(z)$ corresponds to a *real* meromorphic differential $d\omega = dz/f(z)$. This representation highlights the conformal invariance of the problem, which allows us to relate the magnetization distributions in one domain $\mathcal{D}$ to those in the other, say, a canonical one. Thus, for considering all the doubly connected domains, which will be our prime example in this paper, it is sufficient to study only a concentric ring (or annulus), which is the canonical domain for the doubly connected case into which all other doubly connected domains can be conformally mapped.

The annulus, which we denote as $A := \{z \in \mathbb{C} : \rho \leqslant |z| \leqslant 1\}$, is defined by its inner radius $0 < \rho < 1$. If our original doubly connected domain $\mathcal{D}$ is not an annulus, the parameter ρ is called the conformal modulus and is uniquely defined in the process of conformal mapping, otherwise it can be arbitrary. Suppose we have a certain meromorphic function $f(z)$, which is a solution of the Riemann-Hilbert problem (with no normal components to the boundary of the annulus), and it has a number of topological singularities: isolated zeros and poles, which may also be located at the boundary.

Let us now find a specific form of such a constraint for the annulus A. We know that there exists a real holomorphic differential $d\eta = \imath\, d\, z/z$ without zeros and poles in A. Once we divide the differential $d\eta$ by $d\omega$, we get a meromorphic function $v(z) = \imath f(z)/z$, which is real on the boundary circles of the annulus and has zeros and poles exactly at the positions of vortices and antivortices of the original magnetization distribution. Slightly rotating the annulus, we can assume that $v(z)$ has no zeros and poles at the straight line segment $[\rho, 1]$. We then have the following identity:

$$\begin{aligned} 0 &= \iint_{A-(v)} d\log[v(z)] \wedge d\log(z) \\ &= -\oint_{\partial\{A-(v)-[\rho,1]\}} \log(z)\, d\log[v(z)], \end{aligned} \tag{3}$$

where $\wedge$ denotes the wedge product. The integration in the first integral goes over the annulus A with excluded small disks around zeros and poles of the function $v(z)$ denoted by (v). It is equal to zero because $dz \wedge dz = 0$. The integration contour for the second integral is illustrated in Fig. 2.

The second equality is due to the Poincaré-Stokes formula (integration by parts). We have to cut the annulus (along the segment $[\rho, 1]$) to single out the branch of $\log(z)$.

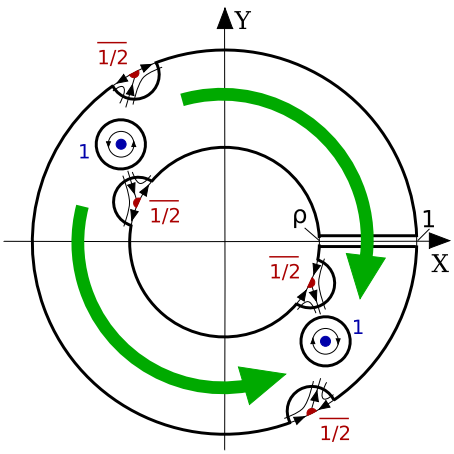

FIG. 2. Integration contour in Eq. (3) for the case of two head-to-head 180° vortex walls in a ring, shown in Fig. 1. Two bold arrows show the general direction of the magnetization inside two magnetic domains. The topological singularities (vortices and antivortices) are shown schematically with their centers marked by bold dots (and half-dots if they are on the boundary). The vortices are labeled with 1 and the half-antivortices at the boundary with $\overline{1/2}$.

On the boundaries of the small disks, including those centered at the boundary of the annulus, the integral is calculated by the residues formula and yields

$$2\pi\imath \sum_{z\in(v)} m(z)\log(z), \tag{4}$$

where z is the coordinate of each zero and pole, and $m(z)$ is the multiplicity of the zero/pole z of the function $f(z)$, negative once z is a pole and taken with the weight $1/2$ if z is on the boundary.

The integral over the boundary circles with excised symmetric vicinities of the boundary vortices is purely imaginary. Finally, the integral over the banks of the slit $[\rho, 1]$ corresponds to integrating the additive jump of the integrand across the banks, which is $-2\pi\imath\, d\log[v(z)]$, along the slit. Since $v(z)$ is real at the slit end points, the real part of this integral lies in the lattice $2\pi^2\mathbb{Z}$, where $\mathbb{Z}$ is the set of integers. Thus, considering only the real part of the identity (3) and dividing both sides by 2π, we get the constraint

$$\mathrm{Arg}(f)_+ - \mathrm{Arg}(f)_- \in \pi\mathbb{Z}, \tag{5}$$

where $\mathrm{Arg}(f)_\pm$ is the sum of the arguments of all zeros/poles of $f(z)$ in the annulus, counted as fractions of 2π, taken with their multiplicities and weighted by $1/2$ if the pole/zero lies at the boundary of the annulus. In other words, the sum of the azimuths of the vortices (counted from the center of the annulus as fractions of 2π) is equal to the sum of azimuths of the antivortices modulo π.

Similar, but more sophisticated, constraints exist also for regions of the higher connectivity, which we plan to explore in our future work. They essentially stem from Abel's theorem for algebraic functions, which implies there should be $c-1$ similar real constraints for positions of zeros and poles, where c is the connectivity of the region. In the simply connected regions, vortices and antivortices do not have such restrictions on their positions.

Another topological constraint we have already explored in our previous work [13] connects the *numbers* of vortices N_V and antivortices N_A (also counted with their multiplicities and taken with the factor $1/2$ if the vortex/antivortex lies at the boundary) in a multiply connected region by the relation $N_A - N_V = c - 2$, where c is again the connectivity of the region. It is not specific for a particular magnetization texture configuration, and it follows from the Hopf-Poincaré theorem about the sum of indexes of singular points of a vector field.

Since all our arguments here and in Ref. [13] are reversible, the inverse statement is also true: in a specific multiply connected region for a given set of singularities satisfying both topological constraints, there always exists a unique (up to a dilation) solution $f(z)$ of the Riemann-Hilbert problem (magnetization texture).

To verify this result, one may check that it holds exactly against all the magnetization distributions in a ring, shown as illustrations in Ref. [13]. Note that, while the resolution of pictures there is rather high, we have performed verification of the constraint (5) using a numerical root-finding technique. The constraint is satisfied exactly up to machine precision (around 10 decimal digits). The experimental verification is more difficult due to the approximate nature of the theory and

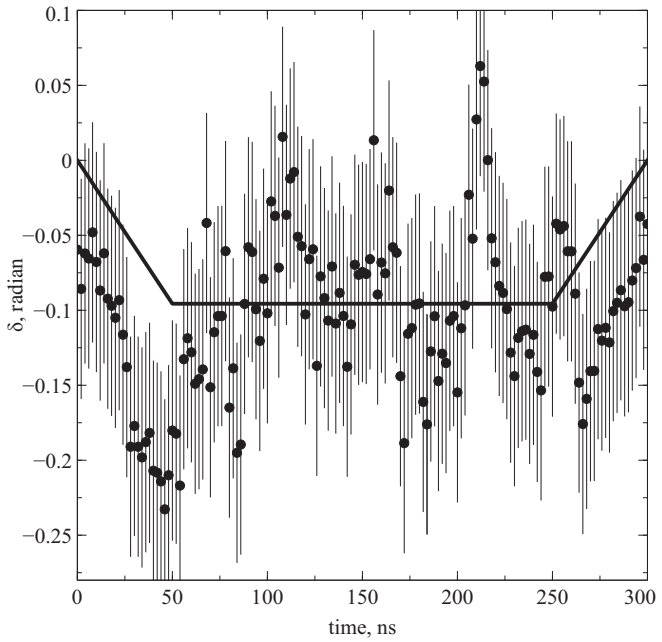

FIG. 3. The dots show the difference of the sums of the azimuth of vortices and antivortices δ as a function of time during the complex dynamical evolution of two vortex walls in a ring, extracted from the experimental data of Ref. [12]. The solid line shows the magnitude of the external field during the evolution in arbitrary units taken with the minus sign for easier comparison. The field is increasing, performing a 360° rotation in the ring plane, then decreasing. The error bars (vertical lines) are computed in the text, taking into account both systematic and statistical errors.

also due to the difficulty in determining the exact topological singularity positions in the relevant nanoscale systems.

Thankfully, there is a recent experiment [12] on vortex domain-wall dynamics in a microscale permalloy ring, which allows us to resolve the positions of vortices (done in the cited paper) and antivortices (done by us) as functions of time, corresponding to the time-varying amplitude and direction of the external field. The computed phase difference $\delta = [\mathrm{Arg}(f)_+ - \mathrm{Arg}(f)_-] \bmod \pi$ is shown in Fig. 3.

The experimental images were acquired stroboscopically, starting from a remanent state, then increasing the magnetic field amplitude, then performing the full rotation of the field (of constant magnitude) in the ring plane, then decreasing the field back to zero, after which the cycle was repeated. They are published as a movie in Supplemental Material to Ref. [12]. The frames of the movie were processed in the original publication by placing the rather large bold dots (with the angular size of about 0.1 rad) on top of magnetic vortices. We have placed similar-sized dots on top of magnetic antivortices and recorded their positions to compute the phase difference δ and plot it in the figure. The updated movie with all the topological singularities marked is available as Supplemental Material [25]. The scatter of the points is substantial and has both random (due to the pinning) and systematic (due to the size of the dots, placed on top of the image) contributions. The random error was estimated by assuming that at a fixed magnitude of the external field, the scatter is entirely due to the random factors, thus the random error of $\sigma_R = 0.0544$ rad was computed as a standard deviation of δ over the time range from 50 to 250 ns. The systematic error $\sigma_S = 0.0493$ rad was taken to be half of the angular size of the vortex-position dot. The error bars of $\sigma = \sqrt{\sigma_R^2 + \sigma_S^2} \simeq 0.08$ rad were estimated by combining these two errors.

The original constraint was derived for the state of remanence (zero applied field). This corresponds to two values of $\delta = -0.06 \pm 0.08$ and 0.04 ± 0.08 at 0 and 300 ns. From this we may directly conclude that the experiment supports our result. However, there is much more information in the data that merits discussion.

First of all, we can see that δ is mostly negative, which means that the antivortices generally move ahead of the vortices during the field cycle. This can be explained by the fact that they are closer to the ends of the magnetic domains, which are directly rotated by the field. The vortex is in between the antivortices and has less traction. The lower traction and the intrinsic pinning on the material and ring thickness imperfections cause the vortex to lag behind, which is just a manifestation of the hysteresis. The deeper the pinning potential is, the larger is the lag. Thus, the presence of pinning implies that δ may assume not just a single value of 0 (as in a perfect material), but a certain range of values, which are selected based on the magnetic history of the sample. For the cyclic magnetization process of Ref. [12] this results in a constant lag.

Another feature of the experimentally measured phase difference in Fig. 3 is that it somehow follows the magnitude of the external field: linearly increasing in magnitude when the field increases (first 50 ns), staying mostly constant (with large fluctuations) when the field magnitude is a constant (between 50 and 250 ns), and linearly decreasing in magnitude when the field is decreased (last 50 ns). The linearity of the δ change in response to the linear change of the field magnitude during the first and last 50 ns indicates to us that there is a static relationship between the δ and the magnitude of the external field. Let us remember that the constraint with $\delta = 0$ (e.g., with no lag of vortices) was derived for a perfect material in zero applied field, assuming the energy hierarchy with the exchange on top and the energy of side and volume magnetic charges at the bottom (of which the energy of side charges was completely eliminated). Once the in-plane magnetic field is taken into account, the Zeeman energy must also find its place in this hierarchy. We know that the field forces the ring to acquire the side magnetic charges (increasing the magnetization component, normal to the ring boundaries). Supposing the field is low enough that the exchange interaction is still dominating, we can retain all the analyticity properties of the function $f(z)$, but we have to reject the assumption that $v(z)$ is real at the boundary of the ring. This means that the contour integral along the boundary circles with excised symmetric vicinities of the boundary vortices is not purely imaginary anymore but has a certain real part, which we will denote as δ_h. In the case of a symmetric circular ring, this real part may depend only on the magnitude of the external field h. Thus, the presence of the external field modifies the constraint by adding the δ_h term. The computation of this term as well as of the effects of pinning may require a substantial extension of the model, and this is beyond the scope of the

present paper. Nevertheless, the presence of both the lag (the constant at $h = 0$ contribution to δ) and the effect of the external field (the field-magnitude-dependent contribution in the case of a circular ring) does not negate the observation that the azimuth of vortices and antivortices during a very complex dynamical evolution of vortex walls in a ring [12] is bound by a constraint due to the fact that the ring is a doubly connected region.

Thus, we have shown that in the multiply connected planar submicron and micron ferromagnetic elements at remanence, there can be topological constraints on vortex and antivortex positions, which arise entirely due to the high connectivity of the region. We have derived the specific form of the constraint for the canonical doubly connected domain, which is a concentric circular ring. The constraint is verified and holds exactly against our earlier analytical solutions [13]. Its existence is also confirmed by the recent experiment on the dynamics of two vortex walls in the ring [12], which additionally demonstrate that restrictions on the vortex movement exist even beyond our original assumptions of zero applied field and the absence of pinning. There are no analogs of such constraints in simply connected elements, where the positions of vortices and antivortices are determined by the least important terms in the energy hierarchy.

Higher element connectivity opens another, largely unexplored, avenue for the design of spintronic devices, since it allows additional means of controlling the magnetization of functional magnetic elements and its dynamics. We hope that understanding the topological restrictions of the vortex/antivortex placement and movement will help in this very interesting and promising endeavor.

The support of the Russian Foundation for Basic Research under the project RFBR 16-01-00568 is acknowledged.

[1] J. Slaughter, Annu. Rev. Mater. Res. **39**, 277 (2009).
[2] A. D. Kent and D. C. Worledge, Nat. Nanotechnol. **10**, 187 (2015).
[3] C. A. Ross, Annu. Rev. Mater. Res. **31**, 203 (2001).
[4] A. Dussaux, B. Georges, J. Grollier, V. Cros, A. Khvalkovskiy, A. Fukushima, M. Konoto, H. Kubota, K. Yakushiji, S. Yuasa *et al.*, Nat. Commun. **1**, 8 (2010).
[5] R. Jansen, J. Phys. D **36**, R289 (2003).
[6] S. S. P. Parkin, M. Hayashi, and L. Thomas, Science **320**, 190 (2008).
[7] N. A. Usov and S. E. Peschany, J. Magn. Magn. Mater. **118**, L290 (1993).
[8] N. A. Usov and S. E. Peschany, Fiz. Met. Metal. (in Russian) **78**(6), 13 (1994).
[9] K. L. Metlov and K. Y. Guslienko, J. Magn. Magn. Mater. **242–245**, 1015 (2002).
[10] K. L. Metlov and Y. P. Lee, Appl. Phys. Lett. **92**, 112506 (2008).
[11] W. Scholz, K. Y. Guslienko, V. Novosad, D. Suess, T. Schrefl, R. W. Chantrell, and J. Fidler, J. Magn. Magn. Mater. **266**, 155 (2003).
[12] A. Bisig, M. Stärk, M.-A. Mawass, C. Moutafis, J. Rhensius, J. Heidler, F. Büttner, M. Noske, M. Weigand, S. Eisebitt, T. Tyliszczak, B. Van Waeyenberge, H. Stoll, G. Schütz, and M. Kläui, Nat. Commun. **4**, 8 (2013).
[13] A. B. Bogatyrev and K. L. Metlov, Low Temp. Phys. **41**, 984 (2015).
[14] F. Schottky, J. Reine Angew. Math. **101**, 227 (1887).
[15] F. Klein, Math. Ann. **36**, 1 (1890).
[16] D. Crowdy and J. Marshall, Computat. Meth. Funct. Theor. **7**, 293 (2007).
[17] K. L. Metlov, Phys. Rev. Lett. **105**, 107201 (2010).
[18] J. W. F. Brown, *Micromagnetics* (Wiley, New York, 1963).
[19] A. Aharoni, *Introduction to the Theory of Ferromagnetism* (Oxford University Press, Oxford, 1996).
[20] K. Y. Guslienko, X. F. Han, D. J. Keavney, R. Divan, and S. D. Bader, Phys. Rev. Lett. **96**, 067205 (2006).
[21] K. L. Metlov, Phys. Rev. Lett. **97**, 127205 (2006).
[22] K. L. Metlov, Phys. Rev. B **88**, 014427 (2013).
[23] C. E. Zaspel, arXiv:1611.00436 [cond-mat.mtrl-sci].
[24] K. L. Metlov, arXiv:cond-mat/0102311.
[25] See Supplemental Material at http://link.aps.org/supplemental/10.1103/PhysRevB.95.024403 for an updated movie with all the topological singularities marked.